Electronic Supplementary Information

Ex-situ upgrading of pyrolysis vapors over $PtTiO_2$: Extraction of apparent kinetics via hierarchical transport modeling

M. Brennan Pecha,*[a] Kristiina Iisa,[a] Michael Griffin,[a] Calvin Mukarakate,[a] Richard French,[a] Bruce Adkins,[b] Vivek S. Bharadwaj,[a] Meagan Crowley,[a] Thomas D. Foust,[a] Joshua A. Schaidle,[a] Peter N. Ciesielski[a]*

[a] National Renewable Energy Laboratory, 15013 Denver W Pkwy, Golden, CO 80401
[b] Oak Ridge National Laboratory, 1 Bethel Valley Rd, Oak Ridge, TN 37830
* Corresponding authors. MBP email Brennan.pecha@nrel.gov; PNC email peter.ciesielski@nrel.gov

Table S1. Ultimate analysis of organic phase of oils (whole oil for pyrolysis only because it is one phase)

Description	Pyrolysis only	Pyrolysis only	0.5% Pt	1% Pt	0.5% Pt	0.5% Pt
B:C, kg/kg	**-**	**-**	**12**	**3**	**6**	**21**
Feed	**CP/FR**	**CP**	**CP/FR**	**CP**	**CP/FR**	**CP/FR**
C	60.8%	56.0%	76.0%	80.4%	76.7%	72.8%
H	6.5%	6.6%	7.6%	7.8%	7.8%	7.4%
N	0.2%	0.2%	0.3%	0.3%	0.3%	0.3%
O (by difference)	32.5%	37.2%	16.1%	11.4%	15.2%	19.5%
H_2O, wt%	19.7%	22.3%	3.0%	4.9%	4.8%	3.7%

GC x GC – TOFMS Analysis

Oil samples were analyzed by two-dimensional gas chromatography with time-of-flight mass spectrometry (GCxGC-TOFMS) using a LECO Pegasus system. Instrument parameters are shown in Table S2. Samples were diluted 1:10 in acetonitrile containing (trifluormethyl)benzene, 2-fluorobiphenyl, and o-terphenyl used as system monitoring compounds. Data analysis was conducted using LECO ChromaTOF version 4.51.6. Quantitation was conducted by applying response factors of representative compound classes detected in catalytic pyrolysis oils. The list of compounds used to calibrate TOF MS response are provided in Table S3. Compounds identified by library search and 2D retention times were binned into their respective compound classes in an Excel spreadsheet. Concentrations were calculated as mass %.

Table S2. Parameters for GC x GC – TOFMS analysis

Column			
Primary	Rtx-5, 10 m x 180 µm x 0.18 µm		
Secondary	DB-1701, 1.0 m x 100 µm x 0.10 µm		
Injector			
1.0 µL injection, split 200:1	300°C		
Oven			
Primary	35°C, hold 7 min, ramp 5°C/min to 255°C		
Secondary	10°C offset from primary		
Modulator	15°C offset from secondary		
Modulator cycle timing	modulator period, sec	hot time, sec	cold time, sec
start-end of runtime	6	1.0	2.0
Mass Spectrometer			
Transfer line	250°C		
TOF mass range	m/z 29-350		
TOF acquisition rate	200 spectra/sec		
Solvent delay	54 s		

Table S3. Compounds used to calibrate TOF MS response

Benzene	p-Cresol
Methyl cyclohexane	o-Methoxyphenol
2,5-Dimethylfuran	Naphthalene
Toluene	Phenanthrene
2-Cyclopenten-1-one	Tetralin
p-Xylene	n-Nonane
1,3,5-Trimethylbenzene	1-Octene
Phenol	n-Decane
2,3-Dihydrobenzofuran	n-Tetradecane
Indene	

CHN and Water Analysis

Oil and aqueous phases and char were analyzed for elemental composition using a LECO TruSpecs CHN analyzer according to ASTM D2591/D5373, and oxygen was calculated by difference for the liquid phases. Water in oil and aqueous phases was determined by Karl Fisher titration.

Packed bed reactor operation parameters and calculated properties

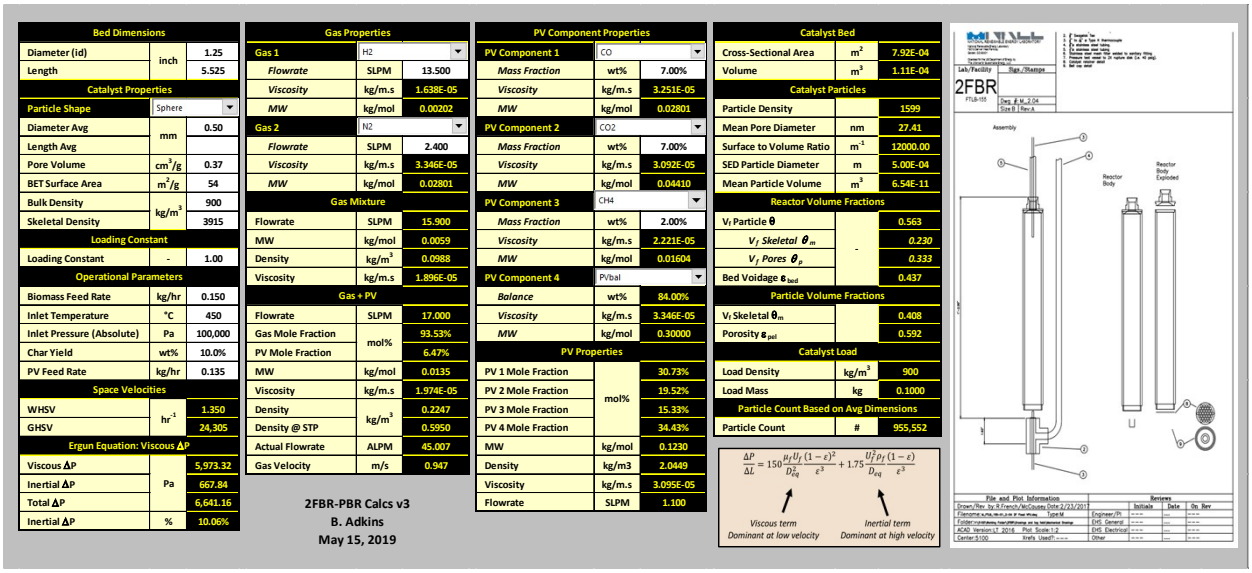

Bed Dimensions		
Diameter (id)	inch	1.25
Length		5.525
Catalyst Properties		
Particle Shape		Sphere
Diameter Avg	mm	0.50
Length Avg		
Pore Volume	cm^3/g	0.37
BET Surface Area	m^2/g	54
Bulk Density	kg/m^3	900
Skeletal Density		3915
Loading Constant		
Loading Constant	-	1.00
Operational Parameters		
Biomass Feed Rate	kg/hr	0.150
Inlet Temperature	°C	450
Inlet Pressure (Absolute)	Pa	100,000
Char Yield	wt%	10.0%
PV Feed Rate	kg/hr	0.135
Space Velocities		
WHSV	hr^{-1}	1.350
GHSV		24,305
Ergun Equation: Viscous ΔP		
Viscous ΔP	Pa	5,973.32
Inertial ΔP		667.84
Total ΔP		6,641.16
Inertial ΔP	%	10.06%

Gas Properties		
Gas 1		H2
Flowrate	SLPM	13.500
Viscosity	kg/m.s	1.638E-05
MW	kg/mol	0.00202
Gas 2		N2
Flowrate	SLPM	2.400
Viscosity	kg/m.s	3.346E-05
MW	kg/mol	0.02801
Gas Mixture		
Flowrate	SLPM	15.900
MW	kg/mol	0.0059
Density	kg/m^3	0.0988
Viscosity	kg/m.s	1.896E-05
Gas + PV		
Flowrate	SLPM	17.000
Gas Mole Fraction	mol%	93.53%
PV Mole Fraction		6.47%
MW	kg/mol	0.0135
Viscosity	kg/m.s	1.974E-05
Density	kg/m^3	0.2247
Density @ STP		0.5950
Actual Flowrate	ALPM	45.007
Gas Velocity	m/s	0.947

2FBR-PBR Calcs v3
B. Adkins
May 15, 2019

PV Component Properties		
PV Component 1		CO
Mass Fraction	wt%	7.00%
Viscosity	kg/m.s	3.251E-05
MW	kg/mol	0.02801
PV Component 2		CO2
Mass Fraction	wt%	7.00%
Viscosity	kg/m.s	3.092E-05
MW	kg/mol	0.04410
PV Component 3		CH4
Mass Fraction	wt%	2.00%
Viscosity	kg/m.s	2.221E-05
MW	kg/mol	0.01604
PV Component 4		PVbal
Balance	wt%	84.00%
Viscosity	kg/m.s	3.346E-05
MW	kg/mol	0.30000
PV Properties		
PV 1 Mole Fraction	mol%	30.73%
PV 2 Mole Fraction		19.52%
PV 3 Mole Fraction		15.33%
PV 4 Mole Fraction		34.43%
MW	kg/mol	0.1230
Density	kg/m3	2.0449
Viscosity	kg/m.s	3.095E-05
Flowrate	SLPM	1.100

Catalyst Bed		
Cross-Sectional Area	m^2	7.92E-04
Volume	m^3	1.11E-04
Catalyst Particles		
Particle Density		1599
Mean Pore Diameter	nm	27.41
Surface to Volume Ratio	m^{-1}	12000.00
SED Particle Diameter	m	5.00E-04
Mean Particle Volume	m^3	6.54E-11
Reactor Volume Fractions		
V_f Particle θ	-	0.563
V_f Skeletal θ_m		0.230
V_f Pores θ_p		0.333
Bed Voidage ϵ_{bed}		0.437
Particle Volume Fractions		
V_f Skeletal θ_m		0.408
Porosity ϵ_{pel}		0.592
Catalyst Load		
Load Density	kg/m^3	900
Load Mass	kg	0.1000
Particle Count Based on Avg Dimensions		
Particle Count	#	955,552

$$\frac{\Delta P}{\Delta L} = 150\frac{\mu_f U_f (1-\varepsilon)^2}{D_{eq}^2 \quad \varepsilon^3} + 1.75\frac{U_f^2 \rho_f (1-\varepsilon)}{D_{eq} \quad \varepsilon^3}$$

Viscous term Dominant at low velocity — *Inertial term Dominant at high velocity*

Figure S1: Operating parameters for the experiments and fluid property calculations.

Microscopy methods and details

Transmission electron tomography was performed to investigate the three-dimensional morphology of intraparticle porosity to inform parameterization of the intraparticle transport model. This technique involves acquiring a series of TEM images at different angles with respect to the electron beam which enables the reconstruction of the 3D sample volume via computational image processing. Slices through the 3D volume obtained using this method are shown at two different magnifications in Figure S2a and b. Due to the large number of images (~160) that are averaged to produce the 3D density field, the contrast between the TiO_2 support and Pt nanoparticles is enhanced with respect to that observed in 2D TEM images. 3D visualizations of the reconstructed volume are shown at two different magnifications in Figure S2 c and d. This analysis reveals that roughly Pt clusters with diameters of roughly 5 nm are well-dispersed on the surface of the support material. The tomographic reconstruction facilities direct quantification of mesoporous dimensions including void space and distribution of pore dimensions. The void volume was determined by first calculating the average and standard deviation of the tomographic density of a clearly indefinable void region within the reconstructed volume. The void fraction of the entire volume was then determining the number of voxels within the volume that displayed a density greater than two standard deviations above the mean density of the void volume. The entire reconstruction was divided into 64 sub-volumes and this calculation was performed within each to determine variability of the void space. By this method the average void fraction was determined to be 57% with a standard deviation of 6.8%. The pore size distribution using a combination of automated computational image transformations.

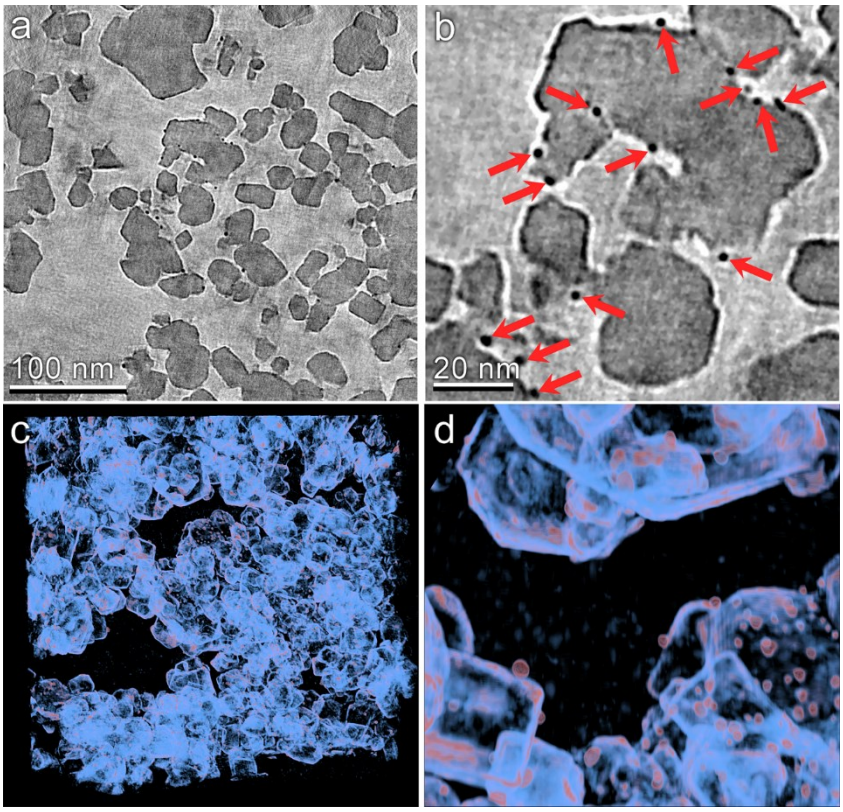

Figure S2. TEM Tomography of the TiO_2 catalyst particle mesostructure. (**a, b**) Slices through the tomographic volume are shown at two different magnifications. Pt particles are clearly identified by their higher electron density (indicated by red arrows in panel b). (**c, d**) 3D visualizations of the reconstructed volume are shown at two different magnifications. Density primarily corresponding to the TiO_2 support is shown as light blue and that roughly corresponding to the Pt particles is shown as orange.

Scanning Electron Microscopy

Whole catalyst particles were mounted on aluminum stubs with conductive carbon adhesive. Samples were imaged without coating using a FEI Quanta 400 FEG using an accelerating voltage of 25 kV.

Transmission Electron Microscopy and Tomography

Catalyst particles were gently crushed and the powder was suspended in ethanol at ~0.5% wt/vol. A volume of 5 µl of the suspension was placed on carbon-coated copper TEM grids with a grid sized of 200 mesh (SPI Supplies, West Chester, PA). Samples were allowed to air dry prior to imaging. A FEI Tecnai G2 20 Twin 200 kV LaB6 TEM (FEI, Hilsboro, OR) instrument was used at an accelerating voltage of 200 kV; images were collected with a Gatan UltraScan 1000 camera (Gatan, Pleasanton, CA). Tomography was performed by first obtaining dual-axis ±60° tilt series of the region of interest at a pixel size of ~0.5 nm. Single axis tomograms were constructed from the tilt series using the R-weighted back projection algorithm and then combined to yield the final reconstruction using the IMOD software package[3]. Tomographic slices were visualized with IMOD the volume reconstruction was visualized with PyMOL[4].

Quantification of Pore Size distribution from TEM Tomography

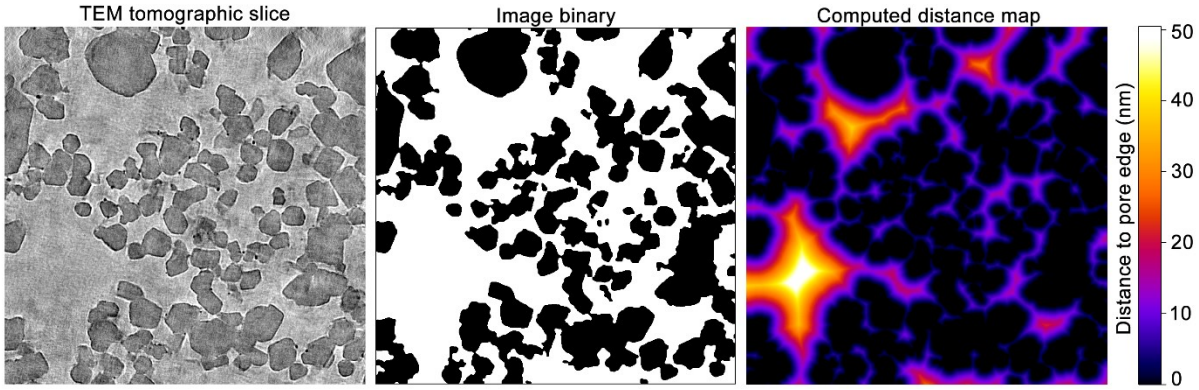

Figure S3. Determination of pore size distribution by computational analysis of TEM tomographic slices. **(Left)** Original tomographic slice used for analysis. **(Center)** Image binary produced from the tomographic slice. **(Right)** Distance map computed from the image binary.

First, an image binary is produced from a tomographic slice by determining a threshold that differentiates the void space from that occupied by the TiO_2 and Pt. Next, a medial axis transform (i.e., skeletonization operation) was computed to determine the centerlines of the filled volume. This transformation was combined with a distance map transform to compute the distance from the center of the void regions to the nearest pore edge. The average pore radius was computed to be 7.82 nm with a standard deviation of 7.84 nm.

Method of lines packed bed reactor model validation

Model validation was performed with method of lines packed bed reactor code as described in the main body of the text for the PtTiO2 vapor phase upgrading. In this simplified case, there is a first order reaction A -> B, 97% conversion with a basic thiele modulus to describe intraparticle reaction-diffusion. Parameters were taken from pg 125 of Rawling's coursework lecture notes,[1] as summarized in Table S4.

Table S4: Parameters used to validate the PBR model

Parameter	*Value*
$r_{catalyst}$	0.003 m (0.3 cm)
T	450 K
P	1.5 atm
$\dot{n}_{A,in}$	12 mol/s
$C_{A,inlet}$	
$k_{intrinsic}$	2.61 s^{-1}
D intra	0.007 cm^2/s
$\rho_{particle}$	0.85 g/cm^3
ρ_{bed}	0.6 g/cm^3
ε_{bed}	1-0.6/0.85 = 0.2941

[1] https://jbrwww.che.wisc.edu/home/jbraw/chemreacfun/ch7/slides-masswrxn.pdf

C_{Asurf}	$c_A = \frac{P}{RT}\frac{N_A}{N_A + N_B}$
$V_{catalystbed}$	1.32 m^3
$V_{voidspace}$	0.55 m^3
V_{rxr}	1.32 m^3
weight catalyst	789 kg
$V_{singlepart}$	1.131E-7 m^3
$n_{catalystparticles}$	11671362.5
$r_{reactor}$	0.3 m
$L_{reactor}$	4.67 m
dn_{part}/dL	1.7647e+06 particles/m

$$R_{Ap} = -\eta k c_{As}$$

$$\Phi = \sqrt{\frac{ka^2}{D_A}}$$

$$\eta = \frac{1}{\Phi}\left[\frac{1}{\tanh 3\Phi} - \frac{1}{3\Phi}\right]$$

a=R/3

Results

The target is for 97% of species A to be converted into species B with this set of parameters. The model achieved this goal with as few as 50 mesh points as shown in table S5.

Table S5

Mesh points	*Species B yield outlet*	*Species A remaining outlet*
100	0.97	0.03
250	0.97	0.03
50	0.9696	0.0301

Calculations for yields of lumped species

Of relevance to this work are the yields of the lumped chemical families across the mass balance of the catalytic VPU. HC indicates hydrocarbons, characterized by detected aromatics, alkanes, alkenes, and C2-C4 light condensables. OX indicates partially deoxygenated organics, characterized by detected cyclopene/anones, phenol, methylphenol, miscellaneous phenols, and furanics. LG is light gas made up of CO, CO2, and CH4. PV_{LMW} is low molecular weight organic fraction of pyrolysis oil that is detectable by GCxGC and is considered reactive on this catalyst. WAT indicates the yield of water produced from PV_{LMW} entering the reactor.

$$HC = \sum_{1:n}^{\text{HC assigned species}} \frac{\overline{x}_{n,\text{org. oil}} \cdot \overline{y}_{oil_{dry}}}{y_{PV_{LMW}}}$$

$$OX = \sum_{1:n}^{\text{OX assigned species}} \frac{\overline{x}_{n,\text{org. oil}} \cdot \overline{y}_{oil_{dry}}}{y_{PV_{LMW}}}$$

$$LG = \sum_{1:n}^{\text{CO, CO}_2\text{, CH}_4} \frac{\overline{y}_{n,\text{catalytic}} - \overline{y}_{n,\text{pyrolysis only}}}{y_{PV_{LMW}}}$$

$$WAT = \frac{\overline{y}_{H_2O,\text{catalytic}} - \overline{y}_{H_2O,\text{pyrolysis only}}}{y_{PV_{LMW}}}$$

$$CK = \frac{\overline{y}_{coke}}{y_{PV_{LMW}}}$$

$$PV_{LMW} = 1 - \left(HC + OX + WAT + CK\right)$$

where

$y_{PV_{LMW}} = \sum \frac{y_{oil}\left(1 - x_{H_2O}\right) - 0.15}{n}$, the average yield of low molecular weight organic pyrolysis vapors considered to be reactive on the catalyst, *y* indicates yield of a fraction from wood, *x* indicates mass fraction of a yield.

The coke: water ratio of 0.67 was estimated based on the elemental analysis of pyrolysis vapors less water which is approximately 56% C, 6.5% H, and 38% O. Some oxygen remains in the char; in general coke has 75% less oxygen than pyrolysis vapors. This is slightly less than the oxygen content of the upgraded pyrolysis vapors, which lose approximately 2/3 of the original oxygen content in the VPU. If this is the case, and all the oxygen is removed in the form of water via dehydration reactions, this corresponds to mass loss of 4% H and 29%, or 33% wt.% H2O. Thus the pyrolysis vapor to coke reaction is assumed to make 67% coke and 33% water. This assumption can be refined in future work if coke characterization is performed.

1. J. T. Miller, M. Schreier, A. J. Kropf and J. R. Regalbuto, *Journal of Catalysis*, 2004, **225**, 203-212.
2. M. Schreier and J. R. Regalbuto, *Journal of Catalysis*, 2004, **225**, 190-202.
3. J. R. Kremer, D. N. Mastronarde and J. R. McIntosh, *Journal of structural biology*, 1996, **116**, 71-76.
4. PyMOL, *The PyMOL Molecular Graphics System*, 2017, **Version 2.0**.